NJC

ROYAL SOCIETY OF CHEMISTRY

PAPER

Cite this: *New J. Chem.*, 2020, **44**, 12793

Aerobic oxidation of 2-aminophenol catalysed by a series of mononuclear copper(II) complexes: phenoxazinone synthase-like activity and mechanistic study†

Nirmalya Podder and Sukanta Mandal *

Three mononuclear copper(II) complexes of types $[Cu(L^1)(Cl)_2]\cdot MeOH$ (**1·MeOH**), $[Cu(L^2)(Cl)_2]\cdot H_2O$ (**2·H_2O**) and $[Cu(L^3)(Cl)_2]$ (**3**) have been synthesized from three reduced Schiff base tridentate N_3 ligands, namely *N*-(pyridin-2-ylmethyl)quinolin-8-amine ($[H_2]L^1$), *N*-(1-methylbenzimidazol-2-ylmethyl)quinolin-8-amine ($[H_2]L^2$), and *N*-(1-methylimidazol-2-ylmethyl)quinolin-8-amine ($[H_2]L^3$), respectively, having variable donor moieties. During metalation all three reduced Schiff base ligands undergo oxidative dehydrogenation *in situ* under aerobic conditions to yield the corresponding Schiff base ligated mononuclear copper(II) complexes. All complexes have been characterized using various spectroscopic techniques such as IR, HRMS-ESI, UV-vis, and EPR. Structural characterization of each complex by single crystal X-ray diffraction reveals that the coordination environment around the copper ion is distorted square pyramidal. The three complexes effectively catalyse the aerial oxidation of 2-aminophenol (H_2AP) to 2-amino-phenoxazine-3-one (APX), thus mimicking the catalytic function of the enzyme phenoxazinone synthase. Kinetic studies have been done to arrive at the following catalytic efficiency order: **3** ≫ **2·H_2O** > **1·MeOH**. The observed trend can be explained by considering the structure–function relation of the catalytic activity. Intramolecular charge distribution (valence tautomerism) within a complex–substrate adduct leads to the generation of a "Cu^I–(substrate radical)" tautomer. This phenomenon has been established by EPR spectroscopy, particularly using 2-anilino-4,6-di-*tert*-butylphenol ($H_2AP^{Ph,t\text{-}Bu}$, a structural analogue of H_2AP) as a substrate. Such a "Cu^I–(substrate radical)" species is believed to promote dioxygen activation. The effects of temperature and pH on the reaction rates have been studied. Activation parameters (E_a, $\Delta H^{\ddagger}$, and $\Delta S^{\ddagger}$) have been evaluated from temperature-dependent kinetic measurements. A plausible reaction pathway has been proposed on the basis of stoichiometry determination, spectroscopic data and kinetic analysis.

Received 20th May 2020,
Accepted 30th June 2020

DOI: 10.1039/d0nj02558e

rsc.li/njc

Introduction

Transition metal complex mediated catalytic oxidations of organic substrates with molecular dioxygen have attracted much attention of researchers during the past few decades.[1–5] These oxidative transformation reactions find applications in chemical industries. Moreover, such reactions mimic the bio functions of certain metalloenzymes that activate dioxygen. In this respect copper-containing enzymes should be particularly mentioned, since they are known to play a crucial role in activating dioxygen and function as monooxygenases, dioxygenases, and oxidases.[6–8] One such oxidative bioprocess of our interest is the oxidase activity of phenoxazinone synthase (PHS).[9–13] PHS is a multicopper enzyme that catalyses the oxidative condensation of two molecules of 3-hydroxy-4-methylanthranilic acid pentapeptide lactone in the presence of dioxygen to form the phenoxazinone chromophore (Fig. 1). This is an important and last step for the biosynthesis of the powerful antineoplastic agent actinomycin D, which is clinically used for the treatment of Wilm's tumors, gestational choriocarcinoma, and other tumor cells.[13] This oxidative condensation reaction of the two substituted 2-aminophenol to phenoxazinone involves six-electron oxidation, which is believed to occur in three consecutive two-electron transfer processes as demonstrated by Begley *et al.*[10]

The crystal structure of PHS from *Streptomyces antibioticus* reveals that the enzyme exists in two oligomeric forms, the dimer and hexamer.[12] The hexameric form shows higher activity

Department of Chemistry, Indian Institute of Technology Kharagpur, Kharagpur 721302, India. E-mail: sukanta.mandal@chem.iitkgp.ac.in

† Electronic supplementary information (ESI) available. CCDC 2001075–2001077. For ESI and crystallographic data in CIF or other electronic format see DOI: 10.1039/d0nj02558e

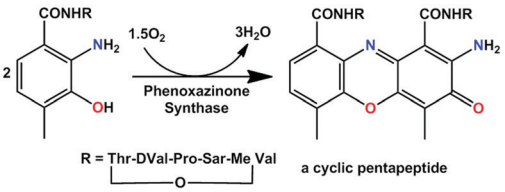

Fig. 1 Phenoxazinone synthase (PHS) reaction; the last step of the biosynthesis of actinomycin D.

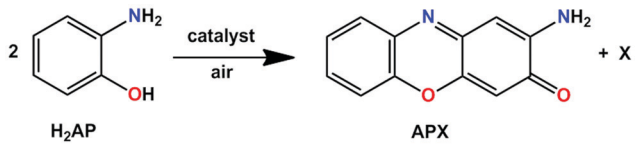

Fig. 3 Model reaction for phenoxazinone synthase: aerial oxidation of 2-amiophenol to 2-amino-phenoxazine-3-one (X represents reduced oxygen species, such as H_2O and/or H_2O_2).

than the dimeric form. Each subunit of the hexamer contains five copper atoms with the presence of all three types of copper-binding motifs: one type-1 (blue), two type-2 (normal) and one binuclear type-3 centres. The schematic diagram of the tetra-copper unit consisting of one type-1, one type-2 and one type-3 is shown in Fig. 2. The fifth copper centre (not shown in the diagram) is located at a distance of ~25 Å from the blue copper and the other normal type-2 copper. On the basis of the coordination environment the fifth copper is assigned as a type-2 centre. This copper centre appears to play an important role to achieve the maximum reactivity of the penta-copper unit by stabilizing the hexameric structure through its interaction between two domains of the enzyme.

With this existing literature knowledge about the structural and functional aspects of PHS, various bioinspired model studies[13–21] have been attempted in past years. The catalytic aerial oxidation of 2-aminophenol (H_2AP) to 2-amino-phenoxazine-3-one (APX) was commonly used as a model reaction to mimic the enzymatic reaction as shown in Fig. 3. However, it is quite challenging to develop a synthetic model complex mimicking all different types of copper sites in one motif. Chaudhuri *et al.* first reported a tetranuclear cubane-like copper(II) core, supported with a redox non-innocent ligand, that could catalyse the aerial oxidation of H_2AP to APX without formation of any non-enzymatic by-product.[14] Afterward a few more tetranuclear cores were developed as PHS mimics.[15] Several heterometallic Cu–Mn cluster compounds were used as functional PHS models.[16] It has been found that dimeric copper(II) complexes could also effectively catalyse the oxidation of H_2AP to APX under aerial conditions.[17] It should be noted that although nature has designed a multi copper active site, conversion of H_2AP to APX can be achieved even by mononuclear metal complexes. In this respect, mononuclear copper[18] and other metal (*e.g.* Mn,[19] Fe,[20] and Co[21]) complexes have been developed as model systems for PHS-like activity. Despite these several literature reports, questions regarding the structure–function relation, mechanism of dioxygen activation and factors affecting the PHS activity remain subjects of interest and require further investigation.

In this endeavour, herein we report the synthesis, characterization and phenoxazinone synthase-like activity of three mononuclear copper(II) complexes of types $[Cu(L^1)(Cl)_2]\cdot MeOH$ (**1·MeOH**), $[Cu(L^2)(Cl)_2]\cdot H_2O$ (**2·H$_2$O**) and $[Cu(L^3)(Cl)_2]$ (**3**) {$[H_2]L^1$ = *N*-(pyridin-2-ylmethyl)quinolin-8-amine; $[H_2]L^2$ = *N*-(1-methylbenzimidazol-2-ylmethyl)quinolin-8-amine; $[H_2]L^3$ = *N*-(1-methylimidazol-2-ylmethyl)quinolin-8-amine}, having N_3-donor ligands with variable donor moieties (Fig. 4). The catalytic activities of the three complexes towards the oxidative coupling of H_2AP to APX have been investigated. To throw light on the mechanistic aspects spectroscopic and kinetic analyses have been performed. The comparative kinetic analysis reveals a

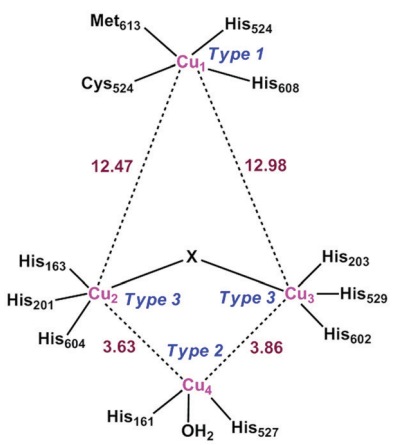

Fig. 2 Schematic diagram of the tetracopper unit and the surrounding ligands of PHS (reproduced from reference 12). X represents an unidentified bridging ligand (supposed to be OH^-). The nonbonding distances between the copper atoms are in units of Å.

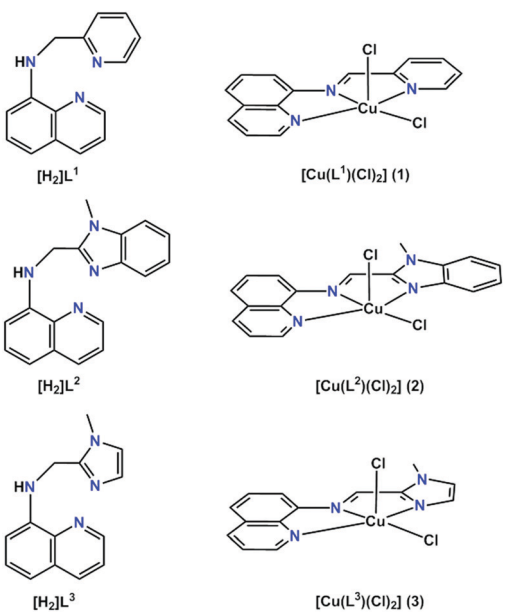

Fig. 4 Ligands and copper(II) complexes considered in this work.

structure–function relation of the catalytic performances (k_{cat}/K_M) of the complexes. In the mechanistic interpretation, valence tautomerization in a complex–substrate adduct leading to equilibration between two redox isomers of types "Cu^{II}–(2-amidophenolato)" and "Cu^{I}–(2-iminosemiquinonato) radical anion" has been proposed to be an important step in the overall catalytic cycle. Such a "Cu^{I}–(substrate radical)" intermediate is considered to be responsible for activation of molecular dioxygen. This phenomenon of valence tautomerism in the complex–substrate adduct was validated by EPR spectroscopy employing 2-anilino-4,6-di-*tert*-butylphenol ($H_2AP^{Ph,t\text{-}Bu}$, an analogue of H_2AP) in particular as a substrate (*vide infra*). Therefore, the present work provides valuable insights towards the mechanistic aspects of phenoxazinone synthase.

Experimental section

Materials and reagents

All reagents were obtained from commercial sources (Sigma Aldrich, Alfa Aesar, TCI Chemicals and Sisco Research Laboratories Pvt. Ltd India) and used as received. Organic solvents were dried/purified prior to use. Milli-Q water (18.2 MΩ) was used to prepare the buffer solutions. 2-(Chloromethyl)-1-methyl-1*H*-benzimidazole[22a] and 2-anilino-4,6-di-*tert*-butylphenol[22b] were prepared following literature procedures.

General instrumentation

C, H, and N analyses were performed using a PerkinElmer Elemental Analyzer (Model No 2400SERIESII). UV-vis spectra were recorded on an Agilent 8454 diode-array spectrophotometer. Infrared (IR) spectra were measured using a PerkinElmer spectrum two FT-IR spectrometer in the 4000–400 cm^{-1} range. High resolution mass spectra (HRMS) were recorded on an Agilent 6545XT AdvanceBio LC/Q-TOF spectrometer. ^{1}H NMR spectra were measured at room temperature on a Bruker 400 Ultrashield (400 MHz) NMR spectrometer; the chemical shifts were reported in ppm referenced to the solvent residual peak. X-Band EPR spectra were measured on a Bruker ELEXSYS 580 spectrometer. The EasySpin[23] software package (version 5.2.28) was used to simulate the EPR spectrum. Purification of water (18.2 MΩ) was done with a Milli-Q system (Millipore, Direct-Q 3 UV). pH was measured by using a Eutech pH tutor. GC-MS analysis was carried out on a Thermo Scientific Trace 1300 gas chromatograph connected to an ISQ single quadrupole MS. The electrochemical analyses of the complexes were performed by using a CH Instruments Electrochemical Analyzer/Workstation Model 660E Series, employing a standard three-electrode cell with a glassy carbon (diameter: 3 mm) working electrode, a platinum-wire auxiliary electrode, and a saturated calomel electrode (SCE) as a reference.

Syntheses of ligands

***N*-(Pyridin-2-ylmethyl)quinolin-8-amine ($[H_2]L^1$).** This ligand was synthesized by slight modification of a published procedure.[24] 8-Aminoquinoline (0.721 g, 5 mmol) was taken in a 100 mL round-bottom flask and dissolved in dry ethanol (30 mL). To it a solution of 2-pyridinecarboxaldehyde (0.536 g, 5 mmol) in ethanol (5 mL) was added dropwise. The resulting reaction mixture was magnetically stirred for 12 hours at room temperature. After that the solvent was removed completely under reduced pressure. The resulting yellow oil residue was dissolved in MeOH (20 mL) and warmed in an oil bath at 45 °C. To it, excess $NaBH_4$ (0.757 g, 20 mmol) was added in small portions over a period of one hour, and then the reaction mixture was stirred for another 12 hours under warm conditions. After evaporation of the solvent completely, the residue was treated with brine solution and the organic components were extracted with 3 × 50 mL of CH_2Cl_2. The combined organic layers were dried over anhydrous $MgSO_4$. Filtration and evaporation of the solvent yielded the crude product as a brown oil. Purification was achieved by column chromatography on silica using a CH_2Cl_2 : MeOH (99 : 1, v/v) mixture to afford 0.825 g of ligand as a reddish-brown thick oil (yield: 70%). ^{1}H NMR (400 MHz, $CDCl_3$, 300 K): δ 8.77 (d, 1H), 8.63 (d, 1H), 8.07 (d, 1H), 7.62 (t, 1H), 7.42–7.37 (m, 2H), 7.32 (t, 1H), 7.18 (t, 1H), 7.07 (d, 1H), 6.99 (br. s, 1H, N–H), 6.61 (d, 1H), 4.72 (d, 2H, –CH_2–).

***N*-(1-Methylbenzimidazol-2-ylmethyl)quinolin-8-amine ($[H_2]L^2$).** A mixture of 8-aminoquinoline (0.721 g, 5 mmol), K_2CO_3 (3.45 g, 25 mmol) and a catalytic amount of KI in MeCN (15 mL) was stirred in a dinitrogen atmosphere. To this a solution of 2-(chloromethyl)-1-methyl-1*H*-benzimidazole (0.903 g, 5 mmol) in MeCN (15 mL) was added dropwise. The reaction mixture was then heated to reflux under a dinitrogen atmosphere for 48 hours. After cooling to room temperature the reaction mixture was filtered through Celite to separate out the solid particles. On evaporation of the solvent to dryness, the crude ligand was obtained as a brown oil. It was then purified by column chromatography on silica using CH_2Cl_2 : MeOH (99 : 1, v/v) as an eluent to afford 0.935 g of ligand as a yellow semi-solid (yield: 65%). ^{1}H NMR (400 MHz, $CDCl_3$, 300 K): δ 8.73 (d, 1H), 8.06 (d, 1H), 7.81 (d, 1H), 7.39–7.25 (m, 5H), 7.12 (d, 1H), 6.94 (d, 1H), 6.78 (br. s, N–H), 4.83 (s, 2H, –CH_2–), 3.87 (s, 3H, –CH_3).

***N*-(1-Methylimidazol-2-ylmethyl)quinolin-8-amine ($[H_2]L^3$).** This ligand was synthesized by a procedure similar to that described for $[H_2]L^1$, but adding 1-methyl-2-imidazolecarboxaldehyde (0.551 g, 5 mmol) instead of 2-pyridinecarboxaldehyde to the reaction mixture. Purification was achieved by a similar method to afford 0.715 g of ligand as a reddish-brown oil (yield: 60%). ^{1}H NMR (400 MHz, $CDCl_3$, 300 K): δ 8.72 (dd, 1H), 8.07 (dd, 1H), 7.41–7.35 (m, 2H), 7.10 (d, 1H), 7.01 (s, 1H), 6.88 (d, 1H), 6.86 (s, 1H), 6.57 (br. s, N–H), 4.60 (d, 2H, –CH_2–), 3.70 (s, 3H, –CH_3).

General synthetic procedure of copper(II) complexes

To a magnetically stirred solution of the respective ligand ($[H_2]L^1$ or $[H_2]L^2$ or $[H_2]L^3$, 0.425 mmol) in methanol (10 mL) was added a methanolic solution (5 mL) of $CuCl_2{\cdot}2H_2O$ (0.425 mmol), resulting in either a green (for the $[H_2]L^1$ and $[H_2]L^3$ ligands) or yellowish-green (for the $[H_2]L^2$ ligand) solution. After 6 hours of stirring under air at room temperature the respective solution was filtered, and addition of diethyl ether to each filtrate initiated the precipitation of solid

products. The individual product was collected by filtration, air dried and dissolved in methanol. Slow diffusion of diethyl ether into the methanol solution of each product yielded the respective complex as a micro-crystalline solid. Single crystals for X-ray diffraction of all three complexes were also obtained by this method. The yields and other physicochemical characterizations of all three complexes are given below.

$[Cu(L^1)(Cl)_2]$·MeOH (1·MeOH). Yield: 0.110 g (65%). Colour: green. Anal. calcd for $C_{16}H_{15}Cl_2CuN_3O$: C 48.07, H 3.78, N 10.51. Found: C 48.12, H 3.65, N 10.56. HRMS-ESI (in MeOH with a trace quantity of HCOOH): *m/z* 296.0251 (calc. 296.0249) $\{[L^1Cu]^+\}$; 330.9933 (calc. 330.9938) $\{[L^1CuCl]^+\}$; 341.0225 (calc. 341.0226) $\{[L^1Cu(HCOO)]^+\}$. UV-vis [λ_{max}, nm (ε, M^{-1} cm^{-1})]: (in MeOH) 655 (180), 440 (2000), 392 (sh) (3680), 368 (5200), 352 (5420), 300 (8200), 280 (sh) (14 930), 258 (sh) (21 950), 230 (33 800). IR (cm^{-1}, selected bands): 3526 (broad), ν(O–H of methanol); 1606 (medium), ν(C═N).

$[Cu(L^2)(Cl)_2]\cdot H_2O$ (2·H_2O). Yield: 0.112 g (60%). Colour: green. Anal. calcd for $C_{18}H_{16}Cl_2CuN_4O$: C 49.27, H 3.68, N 12.77. Found: C 49.21, H 3.56, N 12.71. HRMS-ESI (in MeOH with a trace quantity of HCOOH): *m/z* 349.0509 (calc. 349.0514) $\{[L^2Cu]^+\}$; 384.0195 (calc. 384.0203) $\{[L^2CuCl]^+\}$; 394.0489 (calc. 394.0491) $\{[L^2Cu(HCOO)]^+\}$. UV-vis [λ_{max}, nm (ε, M^{-1} cm^{-1})]: (in MeOH) 664 (142), 490 (sh) (775), 435 (sh) (2515), 410 (2990), 370 (sh) (2445), 314 (2725), 280 (11 166), 272 (11 750), 232 (20 406), 206 (44 903). IR (cm^{-1}, selected bands): 3376 (broad), ν(O–H of water); 1615 (medium), ν(C═N).

$[Cu(L^3)(Cl)_2]$ (3). Yield: 0.090 g (57%). Colour: green. Anal. calcd for $C_{14}H_{12}Cl_2CuN_4$: C 45.36, H 3.26, N 15.11. Found: C 45.42, H 3.18, N 15.16. HRMS-ESI (in MeOH with a trace quantity of HCOOH): *m/z* 299.0356 (calc. 299.0358) $\{[L^3Cu]^+\}$; 334.0041 (calc. 334.0047) $\{[L^3CuCl]^+\}$; 344.0332 (calc. 344.0335) $\{[L^3Cu(HCOO)]^+\}$. UV-vis [λ_{max}, nm (ε, M^{-1} cm^{-1})]: (in MeOH) 652 (125), 475 (2880), 364 (2230), 310 (sh) (760), 285 (sh) (10 100), 263 (16 040), 210 (25 600). IR (cm^{-1}, selected band): 1604 (medium), ν(C═N).

X-ray crystallography

Single-crystal X-ray diffraction data were collected on a Bruker SMART APEXII CCD diffractometer with graphite-monochromated Mo-Kα (λ = 0.71073 Å) radiation. The data for complexes **1·MeOH** and **3** were collected at 120(2) K, whereas the data for complex **2·H_2O** were collected at 296(2) K. Data reduction was performed by using the ''Bruker Saint Plus'' program. Corrections for Lorentz and polarization effects were made. An empirical absorption correction (SADABS v.2.10) was applied. Structures were solved by SIR-2014 and refined by full-matrix least squares methods based on F^2 using SHELXL-2014/7, incorporated in the WinGX 2014.1 crystallographic collective package.[25] All non-hydrogen atoms for both the complexes were refined anisotropically. The positions of the imine –N═C*H*– hydrogen atom for all three complexes and the solvent methanol O–H hydrogen atom for **1·MeOH** were located from difference Fourier maps. The hydrogen atoms of the solvent water molecule for **2·H_2O** could not be located; therefore, the refinement of the oxygen atom was done without hydrogen atoms joined to it. The positions of the remaining hydrogen atoms for all three complexes were calculated assuming ideal geometries. The quality of the crystal data for **2·H_2O** and **3** was poor and a few residual Q-peaks could not be modelled for both the crystals. A summary of pertinent crystallographic parameters of complexes **1·MeOH**, **2·H_2O** and **3** is presented in Table 1.

Table 1 Data collection and structure refinement parameters for **1·MeOH**, **2·H_2O** and **3**

	1·MeOH	**2·H_2O**	**3**
CCDC	2001075	2001076	2001077
Chemical formula	$C_{16}H_{15}Cl_2CuN_3O$	$C_{18}H_{16}Cl_2CuN_4O$	$C_{14}H_{12}Cl_2CuN_4$
Formula weight	399.75	438.80	370.72
Crystal colour	Green	Green	Green
Temperature (K)	120(2)	296(2)	120(2)
Crystal system	Monoclinic	Triclinic	Monoclinic
Space group	*P*21/*c* (no. 14)	*P*$\bar{1}$ (no. 2)	*P*21/*c* (no. 14)
a (Å)	9.575(5)	8.706(6)	6.7255(19)
b (Å)	8.789(5)	9.442(8)	23.788(7)
c (Å)	19.045(5)	11.725(9)	9.162(3)
α (°)	90	94.12(5)	90
β (°)	96.140(5)	98.00(4)	102.396(10)
γ (°)	90	109.84(5)	90
V/(Å^3)	1593.5(13)	890.5(12)	1431.6(7)
Z	4	2	4
D_c (g cm^{-3})	1.666	1.629	1.720
μ (mm^{-1})	1.712	1.541	1.895
Reflections measured	18 945	7704	16 657
Unique reflections [R_{int}]	3246 [0.0904]	3127 [0.0408]	2890 [0.1366]
Number of reflections used [$I > 2\sigma(I)$]	2163	2333	1908
Number of parameters	217	240	195
Final *R* indices	R_1 = 0.0503;[a] wR_2 = 0.1189[b]	R_1 = 0.0777;[a] wR_2 = 0.2084[b]	R_1 = 0.0661;[a] wR_2 = 0.1539[b]
R indices (all data)	R_1 = 0.0884;[a] wR_2 = 0.1351[b]	R_1 = 0.1000;[a] wR_2 = 0.2289[b]	R_1 = 0.1064;[a] wR_2 = 0.1730[b]
Goodness-of-fit on F^2	1.009	1.041	1.000
Largest residual peak and hole (e Å^{-3})	0.784 and −0.625	1.211 and −0.691	1.339 and −1.093

[a] $R_1 = \sum(|F_o| - |F_c|)/\sum|F_o|$. [b] $wR_2 = \{\sum[w(|F_o|^2 - |F_c|^2)^2]/\sum[w(|F_o|^2)^2]\}^{1/2}$.

Kinetic experiments

The phenoxazinone synthase-like activities of complexes **1·MeOH**, **2·H_2O**, and **3** were studied using 2-aminophenol (H_2AP) as a model substrate. The oxidation of H_2AP was performed under aerobic conditions in the presence of the respective complex in a water–methanol (H_2O : MeOH = 67 : 33, v/v) solvent mixture. The solution was buffered using HEPES (for pH 7.00–8.00) or CHES (for pH 8.50–10.00). In all cases the buffer strength was maintained at 100 mM. A correction of 0.051 pH units was subtracted from the measured pH reading to compensate the methanol–water liquid junction potential.[26] The kinetic experiments for the oxidation of H_2AP were carried out spectrophotometrically using an Agilent 8454 diode array UV-vis spectrophotometer, equipped with a thermostatic water circulator (Julabo, Model: Corio CD-200F). The progress of the reaction was monitored by following the increase of the characteristic absorption band of the product 2-amino-phenoxazine-3-one (APX) at 440 nm (ε = 18 300 M^{-1} cm^{-1})[27] as a function of time. Experiments to determine the dependence of the rate on the substrate concentrations and various kinetic parameters were carried out at 30 °C at pH 8.6, $[complex]_0 = 2.5 \times 10^{-5}$ M, $[H_2AP]_0 = 1.25 \times 10^{-4}$ to 12.5×10^{-4} M, for all three complexes. The initial rate method was used to analyse the kinetic data. In order to study the effect of catalyst concentration on the reaction rate, kinetic experiments were performed at 30 °C at pH 8.6 keeping the H_2AP concentration (3.75×10^{-3} M) fixed and varying the complex concentrations from 2.5×10^{-5}–7.5×10^{-5} M. To determine the activation parameters the catalytic reactions for all three complexes were performed in a temperature range from 298 K to 313 K at pH 8.6 with $[complex]_0 = 2.5 \times 10^{-5}$ M and $[H_2AP]_0 = 12.5 \times 10^{-4}$ M. The first order rate constants at different temperatures were calculated by dividing the initial rates by the concentration of catalyst used. To examine the effect of pH on the catalytic reaction, kinetic experiments were performed at various pH from 7.5 to 9.6 at 30 °C with $[complex]_0 = 2.5 \times 10^{-5}$ M and $[H_2AP]_0 = 12.5 \times 10^{-4}$ M. In all of these experiments, blank studies for auto aerial oxidation of the substrate without addition of the catalyst were performed. The rate of auto-oxidation was found to be negligible in all cases, and therefore was ignored.

Reaction product analysis

GC-MS. The oxidation reactions of 2-aminophenol ($[H_2AP]_0 = 2.5 \times 10^{-3}$ M) in the presence of **1·MeOH**, **2·H_2O**, and **3** ($[complex]_0 = 2.5 \times 10^{-4}$ M) were carried out in a methanol–water buffer mixture (pH 8.6) at room temperature. After 2 h, the solvent was removed completely from each catalytic reaction. The organic substances were extracted with CH_2Cl_2. Evaporation of the solvent yielded a reddish-brown residue which was subjected to GC-MS analysis using methanol as an eluent and He as a carrier gas. 2-Amino-phenoxazine-3-one (APX) was found to be a major product in all three catalytic reactions.

^{1}H NMR. The formation of 2-amino-phenoxazine-3-one (APX) during the catalytic reaction was also identified by ^{1}H NMR spectroscopy. The oxidation reactions of 2-aminophenol ($[H_2AP]_0 = 2.5 \times 10^{-2}$ M) in the presence of three different catalysts ($[complex]_0 = 2.5 \times 10^{-3}$ M) were carried out in a methanol–water buffer mixture (pH 8.6) at room temperature. After 5 hours, the organic products were extracted with 3 × 10 mL of CH_2Cl_2. The combined CH_2Cl_2 layers were washed with saturated brine solution and dried over anhydrous Na_2SO_4. Filtration followed by removal of the solvent yielded a brown residue, which was identified by ^{1}H NMR. ^{1}H NMR data for 2-amino-phenoxazine-3-one (APX), (400 MHz, $CDCl_3$, 300 K): δ 7.77–7.75 (m, 1H), 7.44–7.37 (m, 3H), 6.48 (s, 1H), 6.42 (s, 1H), 5.13 (br. s, 2H).

Detection and quantification of hydrogen peroxide in the catalytic reactions

The detection and quantification of hydrogen peroxide during the catalytic reactions in the presence of **1·MeOH**, **2·H_2O**, and **3** was done by iodide titration. Since H_2O_2 decomposes readily in basic medium, to detect the presence of H_2O_2 in the catalytic solutions experiments were carried out in a non-buffered 33% MeOH–H_2O solvent mixture with $[complex]_0 = 2.5 \times 10^{-5}$ M and $[H_2AP]_0 = 7.5 \times 10^{-4}$ M. The progress of the reaction was followed spectrophotometrically for 1 h. The amount of oxidised product (2-amino-phenoxazine-3-one, APX) formed in each catalytic reaction was quantified by the absorption spectra (λ = 440 nm, ε = 18 300 M^{-1} cm^{-1}).[27] After that, each solution was acidified by adding H_2SO_4 to pH ≈ 2 to stop further oxidation, and the solution was treated with excess KI and a catalytic amount of ammonium molybdate. The concentration of hydrogen peroxide was measured by determining the amount of I_3^- ions formed (as per the reactions $H_2O_2 + 2I^- + 2H^+ \rightarrow 2H_2O + I_2$; $I_{2(aq)} + I^- \rightarrow I_{3(aq)}^-$) using the absorption spectrum (λ_{max} of I_3^- = 353 nm; ε = 26 000 M^{-1} cm^{-1}).[28] The concentration of H_2O_2 corresponds to the amount of APX generated at the end of the reaction for each catalytic reaction. A controlled blank study (without catalyst) was also performed. No significant I_3^- band was observed during the blank test.

Results and discussion

Design, synthesis and characterization

In order to elucidate the structure–function relation of the reactivity, it is necessary to design ligands with variation of the donor moieties in a systematic fashion. Towards this goal, three tridentate N_3 donor ligands $[H_2]L^1$, $[H_2]L^2$ and $[H_2]L^3$, bearing a common 8-aminoquinoline moiety but varying the third donor moiety from pyridyl to benzimidazole to imidazole, respectively, have been designed. It is anticipated that all three ligands would adopt a similar binding motif with the metal centre (same geometry), but they would create variable stereochemical properties by virtue of the diverse donor ability and steric influence.

The ligands $[H_2]L^1$ and $[H_2]L^3$ were synthesized following similar methodology. In a typical reaction 1 : 1 condensation of 8-aminoquinoline with 2-pyridinecarboxaldehyde or 1-methyl-2-imidazolecarboxaldehyde produced the respective Schiff base products as a mixture of *E* and *Z* isomers, which upon further

reduction with $NaBH_4$ in methanol afforded the corresponding reduced Schiff base products $[H_2]L^1$ and $[H_2]L^3$. The ligand $[H_2]L^2$ was synthesized in one-pot by reacting 8-aminoquinoline with 2-(chloromethyl)-1-methyl-1*H*-benzimidazole in the presence of K_2CO_3 as a base and a catalytic amount of KI under reflux conditions in MeCN. After purification all three ligands were obtained in moderately good yield. The ligands were characterized by ^{1}H NMR spectroscopy (see Fig. S1–S3 in the ESI†). The reaction of $CuCl_2{\cdot}2H_2O$ with the reduced Schiff base ligands $[H_2]L^1$, $[H_2]L^2$ and $[H_2]L^3$ in a 1 : 1 molar ratio in methanol promoted metal-mediated oxidative dehydrogenation[29] of the ligands under aerobic conditions to form the corresponding Schiff base ligated mononuclear copper(II) complexes, $[Cu(L^1)(Cl)_2]{\cdot}$MeOH (**1·MeOH**), $[Cu(L^2)(Cl)_2]{\cdot}H_2O$ (**2·H$_2$O**) and $[Cu(L^3)(Cl)_2]$ (**3**). Elemental analysis (C, H, and N) data show good agreement with the above formulations for all three complexes. The complexes were characterized by various spectroscopic techniques (*viz.* IR, HRMS, UV-vis, and EPR) along with structural analyses.

Description of structures

Single crystal X-ray diffraction analyses reveal that **1·MeOH**, **2·H$_2$O** and **3** are monomeric compounds with similar structural features. The ORTEP diagrams of the monomeric units are presented in Fig. 5. Selected bond lengths and the bond angles are listed in Table 2. The penta-coordination polyhedron around the Cu(II) ion in each complex can be best described as square pyramidal with τ values 0.07 (**1·MeOH**), 0.05 (**2·H$_2$O**) and 0.16 (**3**) [τ = 0 for an ideal square pyramid, and 1 for an ideal trigonalbipyramid, as defined by Addison[30] *et al.*]. In all complexes, the three equatorial positions are occupied by nitrogen donor groups of the respective tridentate ligand, whereas the fourth equatorial and the axial positions are occupied by two chloride ions. In each complex the Cu(II) ion is found to deviate from the equatorial plane. The displacement (Δd) from the least-squares plane of the equatorial atoms N(1), N(2), N(3), and Cl(2) is measured to be 0.3474(3) Å (**1·MeOH**), 0.3328(8) Å (**2·H$_2$O**) and 0.2669(1) Å (**3**). In each complex all the three Cu–N distances are nearly comparable; however, the equatorial Cu(1)–Cl(2) is slightly longer than the other three Cu–N bonds. This is in accordance with the higher van der Waals radii of the chloride ion. The axial Cu(1)–Cl(1) bond is relatively longer compared to the equatorial bonds for each complex. This axial elongation is a consequence of the Jahn–Teller distortion expected for d^9 Cu(II) ions. The angles around Cu(II) centres in all complexes deviate from the ideal square pyramidal angles, implying that the coordination spheres about Cu(II) ions are distorted in all cases (Table 2). The C(10)–N(2) bond distances for all three complexes [1.287(5) for **1·MeOH**; 1.211(10) for **2·H$_2$O** and 1.305(7) for **3**] are typical of a carbon–nitrogen double bond, affirming the formation of an imine (C=N) bond.

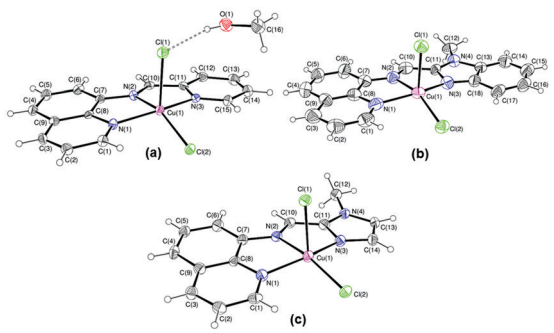

Fig. 5 ORTEP (30%) view of complexes (a) $[Cu(L^1)(Cl)_2]{\cdot}$MeOH (**1·MeOH**), (b) $[Cu(L^2)(Cl)_2]{\cdot}H_2O$ (**2·H$_2$O**) and (c) $[Cu(L^3)(Cl)_2]$ (**3**). The solvent water molecule is not shown for **2·H$_2$O**. The small circles represent the hydrogen atoms (not labelled).

Table 2 Selected bond lengths (Å) and bond angles (°) of **1·MeOH**, **2·H$_2$O** and **3**

	1·MeOH	**2·H$_2$O**	**3**
Cu(1)–N(1)	2.021(3)	2.085(8)	2.046(5)
Cu(1)–N(2)	1.993(3)	2.078(7)	2.005(4)
Cu(1)–N(3)	2.037(4)	1.980(7)	2.022(5)
Cu(1)–Cl(2)	2.2505(13)	2.243(2)	2.2467(16)
Cu(1)–Cl(1)	2.5164(16)	2.499(3)	2.5313(16)
C(10)–N(2)	1.287(5)	1.211(10)	1.305(7)
N(1)–Cu(1)–N(2)	80.67(14)	76.2(3)	79.77(19)
N(1)–Cu(1)–N(3)	158.50(14)	154.6(3)	156.08(17)
N(2)–Cu(1)–N(3)	79.56(14)	80.4(3)	80.04(19)
N(1)–Cu(1)–Cl(1)	97.73(11)	95.6(2)	93.35(13)
N(1)–Cu(1)–Cl(2)	96.78(10)	96.5(2)	98.91(14)
N(2)–Cu(1)–Cl(1)	97.09(11)	98.51(19)	90.11(13)
N(2)–Cu(1)–Cl(2)	154.45(11)	157.5(2)	165.67(13)
N(3)–Cu(1)–Cl(1)	93.01(11)	97.5(2)	99.39(13)
N(3)–Cu(1)–Cl(2)	97.40(10)	101.4(2)	97.48(14)
Cl(1)–Cu(1)–Cl(2)	108.43(5)	103.45(9)	104.21(6)

Spectroscopic characterization

The IR spectra of all three complexes are depicted in Fig. S4–S6 (ESI†). A moderately strong band at 1606 cm^{-1} (for **1·MeOH**), 1615 cm^{-1} (for **2·H$_2$O**) and 1604 cm^{-1} (for **3**) due to the ν(C=N) stretching vibration of the coordinated ligand was observed. The observed trend of the stretching frequency values **2·H$_2$O** > **1·MeOH** > **3** can be rationalized based on the relative bond strength of the imine moiety of the complexes as determined from the X-ray analysis. In fact, we have found a good correlation between the ν(C=N) stretching frequency values and the C=N bond lengths of the complexes as shown in Fig. S7 (ESI†). In the spectrum of **1·MeOH**, a broad band at 3526 cm^{-1} corresponding to ν(OH) of the solvated methanol was also observed. This band appears at lower frequency compared to the free methanol. Such lowering could be explained by the participation of the O–H group of methanol in the formation of a strong inter-molecular hydrogen bond with the chloride ion, as depicted in Fig. 5a. For **2·H$_2$O** a broad band due to the ν(OH) stretching vibration of the solvated water molecule was found at 3376 cm^{-1}.

The HRMS spectra of all complexes in methanol show similar patterns. The spectral data authenticate the formation of a 1 : 1 metal–ligand complex in all cases. As shown in Fig. S8, S9 and S10 (ESI†) the major peaks found correspond to the species $[LCu]^+$, $[LCuCl]^+$, and $[LCu(HCOO)]^+$ (where L = L^1 or L^2 or L^3 for complexes **1·MeOH** or **2·H$_2$O** or **3**, respectively).

The calculated *m/z* values of all species are in good agreement with the experimentally observed *m/z* values (see the Experimental section).

The electronic spectra of the complexes in methanol are displayed in Fig. S11–S13 (ESI†). In the visible region a low intensity band at 655 nm for **1·MeOH**, 664 nm for **2·H$_2$O**, and 652 nm for **3** due to d–d transitions was observed. This spectral feature is consistent with a five-coordinate square pyramidal geometry for the Cu(II) ion.[31a] For all three complexes the lower wavelength region is dominated by several charge transfer bands. The $Cl^- \rightarrow Cu(II)$ charge transfer bands were observed in a range of 350–490 nm, whereas the intra-ligand charge transfer bands ($\pi \rightarrow \pi^*$, $n \rightarrow \pi^*$ *etc.*) were found in a range of 205–310 nm for all complexes.

The X-band EPR spectra of the copper(II) complexes **1·MeOH**, **2·H$_2$O** and **3** in methanol were recorded at 298 K and 77 K. All three complexes show almost similar spectral features at both temperatures. Representative experimental and simulated spectra for **1·MeOH** are shown in Fig. S14 (ESI†). At 298 K the methanol solution of copper(II) complexes showed an isotropic signal with four well resolved copper hyperfine resonances (g_{iso} = 2.127, A_{iso} = 72.8 G). At 77 K the spectra of the methanolic solution of all three complexes are axial type ($g_\parallel > g_\perp > 2$) where hyperfine splitting was observed with $g_\parallel$ signal ($g_\parallel$ = 2.23, $g_\perp$ = 2.083, $A_\parallel$ = 181 G, $A_\perp$ = 16.5 G). This axial pattern is characteristic of a square pyramidal mononuclear Cu(II) compound having an unpaired electron in the $d_{x^2-y^2}$ orbital.[31b]

Electrochemical study

In order to know the donor effect of the ligand the electrochemical properties of complexes **1·MeOH**, **2·H$_2$O** and **3** were measured by cyclic voltammetry in methanol. As shown in Fig. S15 (ESI†) all three complexes show irreversible cathodic reduction peaks, which are tentatively assigned as the Cu^{II}/Cu^{I} redox potential. The irreversible nature of the cyclic voltammogram is probably due to the large structural change (from square pyramidal to distorted tetrahedral) upon the reduction of copper(II) to copper(I). The E_{Pc} values were measured to be −0.12 V, −0.06 V and −0.10 V *vs.* SCE for **1·MeOH**, **2·H$_2$O** and **3**, respectively. The closely similar E_{Pc} values imply that all three ligands possess analogous donor properties.

Phenoxazinone synthase-like activities and kinetic studies

The phenoxazinone synthase-like activities of **1·MeOH**, **2·H$_2$O** and **3** were examined by following the oxidative dimerization reaction of 2-aminophenol (H_2AP) to 2-amino-phenoxazine-3-one (APX) under aerobic conditions at 30 °C. A methanol–water solvent mixture (33%, v/v; pH 8.6) was chosen as the reaction medium to resemble physiological conditions. The catalytic reactions were assessed by monitoring the increase in the characteristic absorption band of the phenoxazinone chromophore at 440 nm (ε = 18 300 M^{-1} cm^{-1})[27] as a function of time. Representative spectral growth over time for complex **3** is shown in Fig. 6. It should be noted that no significant growth of the 440 nm band was observed under anaerobic conditions,

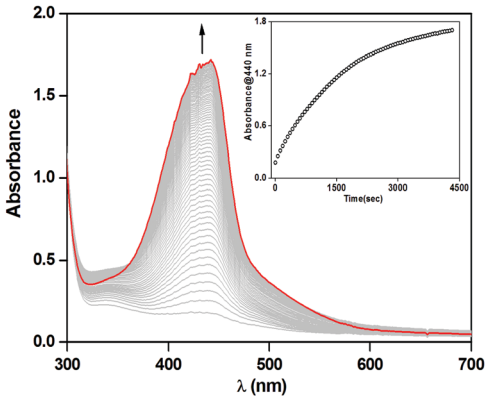

Fig. 6 Formation of the phenoxazinone chromophore band at 440 nm due to aerobic oxidation of H_2AP in the presence of complex **3** (conditions: $[\mathbf{3}]_0$ = 2.5 × 10^{-5} M and $[H_2AP]_0$ = 12.5 × 10^{-4} M) in air-saturated MeOH–H_2O (33%, v/v; pH 8.6, 30 °C). Inset plot: Growth of the 440 nm band over time.

implying that molecular dioxygen is necessary to bring about the oxidative transformation reaction. The GC-MS and ^{1}H NMR (Fig. S16 and S17, respectively, ESI†) analyses indicated the formation of APX as a major product in all three cases. It has been found that all three complexes are active catalysts for the aerial oxidation of H_2AP to APX.

To evaluate the extent of the catalytic efficiency of the complexes kinetic experiments were performed under excess substrate conditions. For a particular catalyst concentration, the plots of initial rates (v_0) *versus* concentration of substrate $[S]_0$ show saturation behaviour for all three complexes as presented in Fig. 7. These saturation kinetics indicate that an intermediate complex–substrate adduct forms in a pre-equilibrium process before the irreversible rate-determining product release step. Primarily, we analysed the data using Michaelis–Menten hyperbolic eqn (1), which has been regularly used for modelling enzymatic saturation kinetics.[32]

$$v_0 = \frac{V_{max}[S]_0}{K_M + [S]_0} \quad (1)$$

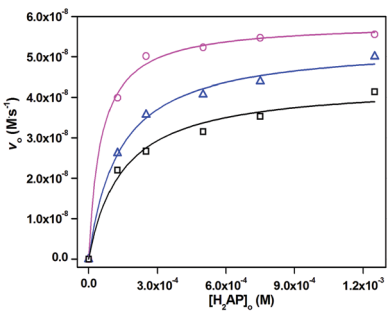

Fig. 7 Dependence of the initial rate on the concentration of H_2AP for the oxidation reaction catalysed by **1·MeOH** (black blocks), **2·H$_2$O** (blue triangles) and **3** (magenta circles). Conditions: $[complex]_0$ = 2.5 × 10^{-5} M, $[H_2AP]_0$ = 2.5 × 10^{-4} to 12.5 × 10^{-4} M, in air-saturated MeOH–H_2O (33%, v/v; pH 8.6, 30 °C). Symbols and solid lines represent the experimental data and theoretical fit (eqn (1)), respectively.

Table 3 Kinetic parameters (obtained from Michaelis–Menten eqn (1)) for the oxidation of H_2AP catalysed by copper(II) complexes at 30 °C in 33% MeOH–H_2O (pH 8.6)

Complex	V_{max} (M s^{-1})	K_M (M)	K_{ass} (M^{-1})	k_{cat} (s^{-1})	k_{cat}/K_M (M^{-1} s^{-1})
1·MeOH	4.35×10^{-8}	14.60×10^{-5}	6.85×10^{3}	174×10^{-5}	12
2·H_2O	5.33×10^{-8}	13.21×10^{-5}	7.57×10^{3}	213×10^{-5}	16
3	5.85×10^{-8}	5.33×10^{-5}	18.76×10^{3}	234×10^{-5}	44

The values of the maximum rate of reaction (V_{max}) and Michaelis binding constant (K_M) were determined by a non-linear fit computer program (Origin 8.5) using eqn (1). The catalytic turnovers (k_{cat}) were calculated by dividing V_{max} by the concentration of the complex used. The catalytic efficiencies *i.e.* second order rate constants were obtained from the k_{cat}/K_M ratio. The kinetic parameters of complexes **1·MeOH**, **2·H_2O** and **3** are summarized in Table 3. To determine the order of reaction with respect to the catalyst concentration, kinetic studies were performed by varying the concentration of the complexes and keeping the substrate concentration fixed. A linear dependency between the initial rates and the complex concentrations was observed for each complex. From the slope of the straight lines in Fig. S18 (ESI†) the rate constants were determined to be 166×10^{-5} s^{-1} (**1·MeOH**), 197×10^{-5} s^{-1} (**2·H_2O**) and 226×10^{-5} s^{-1} (**3**). The first-order dependence of the rate with respect to the catalyst confirms that a single copper(II) complex is involved in each catalytic reaction.

The catalytic efficiencies for the oxidation of H_2AP follow the order **3** ≫ **2·H_2O** > **1·MeOH** (Table 3). The catalytic performances of the three complexes are comparable with the previously reported copper(II) complexes.[13–15,17,18] In an oxidase-type enzymatic reaction, complex–substrate adduct formation and activation of molecular dioxygen are considered to be crucial steps in the catalytic process. During oxidation of H_2AP, the copper(II) centre undergoes reduction to the copper(I) state *via* intramolecular electron transfer from the bound substrate to the copper(II) centre; molecular dioxygen then reacts with the reduced copper(I) to regenerate the copper(II) state, which again is involved in the catalytic cycle (*vide infra*). Therefore, it is understandable that the catalytic reactivity would depend on two factors: (i) the extent of complex–substrate adduct formation and (ii) the ease of dioxygen activation. Since the Cu^{II}/Cu^{I} redox potentials of the present three complexes are very similar, the observed difference in reactivity may not be due to the reactivity difference of copper(I) species with dioxygen; rather it is mostly because of the difference in complex–substrate binding affinity. The complex–substrate binding constant (K_{ass}) can be determined from the reciprocal of the Michaelis constant, K_M ($K_{ass} = 1/K_M$) – the higher the value of K_{ass} the greater is the binding affinity. From Table 3 it is found that the binding affinities of the complexes with the substrate follow the order **3** ≫ **2·H_2O** > **1·MeOH**. Several factors need to be considered to assess the order of the binding affinity of the three complexes with the substrate, such as the stereochemical properties, exogenous donor's property and steric match. We found a good correlation between the deviation of the copper(II) ion (Δd) from the mean equatorial plane and the binding constant, K_{ass} (or catalytic efficiency, k_{cat}/K_M). As shown in Fig. 8 the K_{ass} value (and consequently k_{cat}/K_M) increases with a decrease in the deviation of the copper(II) ion from the mean equatorial plane. Smaller deviation of the copper centre from the equatorial plane leads to a better overlap between metal orbitals and ligand (substrate) orbitals, which would favour the formation of a stable complex–substrate adduct. Therefore, the observed trend of catalytic performances **3** ≫ **2·H_2O** > **1·MeOH** is accountable by considering the structure–function relation of the reactivity.

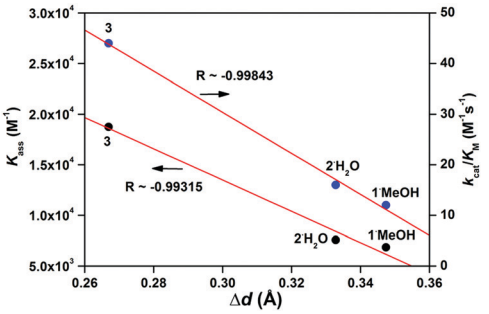

Fig. 8 Correlation between the deviation of the copper(II) ion (Δd) from the mean equatorial plane and the binding constant, K_{ass} (or catalytic efficiency, k_{cat}/K_M), for the copper(II) complexes **1·MeOH**, **2·H_2O** and **3**.

Stoichiometry and fate of dioxygen

The dimerization of 2-aminophenol (H_2AP) to 2-aminophenoxazine-3-one (APX) involves a six-electron oxidation process, where dioxygen acts as a terminal electron acceptor. In this process dioxygen could be reduced either to water (four-electron reduced enzymatic by-product) or H_2O_2 (two-electron reduced non-enzymatic by-product) or both. The formation of H_2O_2 could be identified by iodide titration. In the present studies an appreciable amount of H_2O_2 accumulation was found for all catalytic reactions performed by the copper(II) complexes. The concentration of H_2O_2 was determined spectrophotometrically by measuring the amount of I_3^- ions generated (λ = 353 nm; ε = 26 000 M^{-1} cm^{-1}, Fig. S19, ESI†).[28] For each catalytic reaction equal amounts of H_2O_2 and APX were found to be generated. Therefore to accomplish the six-electron oxidation process, two dioxygen molecules are required. Understandably, out of two dioxygen molecules, if one is reduced to H_2O_2, then the other must be converted to two molecules of water. Hence the stoichiometry of the reaction can be represented by the equation as shown in Fig. 9.

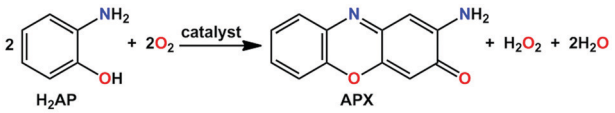

Fig. 9 Stoichiometric equation of aerial oxidation of 2-amiophenol to 2-amino-phenoxazine-3-one catalysed by the copper(II) complexes.

Valence tautomerism in the complex–substrate adduct and EPR studies

2-Amidophenoxide, being a prototype redox non-innocent ligand, is known to exhibit charge distribution with redox active transition metal ions, leading to formation of valence tautomers.[33] To shed light on this aspect for the present studies, all copper(II) complexes were treated with five equivalents of 2-aminophenol under anaerobic conditions in methanol and the reaction solutions were analysed by EPR spectroscopy at 298 K. Exclusion of dioxygen from the reaction conditions allows us to focus only on the initial binding step of the complex and substrate to elucidate the electronic structure of the complex–substrate adduct. In each case, we observed a reduction of Cu(II) signal ($g_{iso} > 2$) intensities after addition of 2-aminophenol. The normalized EPR spectra of **1·MeOH** and after treating with 2-aminophenol are shown in Fig. S20 (ESI†) for illustration. This finding implies that a certain portion of Cu(II) was reduced to the Cu(I) state by the substrate. Since both copper(II) and 2-amidophenoxide (AP^{2-}) are redox non-innocent in nature, a strong redox interaction among them can be envisioned in the complex–substrate adduct, Cu^{II}–(2-amidophenolato) $\{\mathbf{Cu^{II}}\text{–}\mathbf{(AP)^{2-}}\}$. Thus facile intramolecular electron transfer from AP^{2-} to the Cu(II)-centre can be anticipated to generate a Cu^{I}–(2-imino-semiquinonato) radical anion $\{\mathbf{Cu^{I}}\text{–}\mathbf{(ISQ)^{\bullet -}}\}$ by valence tautomerism. Therefore, in the present studies, a decrease of the Cu(II) signal intensities can be realized by considering an equilibrium between two valence tautomers: $\{\mathbf{Cu^{II}}\text{–}\mathbf{(AP)^{2-}}\}$ and $\{\mathbf{Cu^{I}}\text{–}\mathbf{(ISQ)^{\bullet -}}\}$. However, the signal for the radical anion species expected at $g \leq 2$ was not detected, probably due to rapid quenching of the radical character because of instability.

To get support for the above proposition of valence tautomerism we choose 2-anilino-4,6-di-*tert*-butylphenol ($H_2AP^{Ph,t\text{-}Bu}$) – an analogue of H_2AP – as a substrate, since it can produce relatively stable radical species. In contrast with substrate H_2AP, the EPR spectra of copper(II) complexes treated with $H_2AP^{Ph,t\text{-}Bu}$ in methanol anaerobically at 298 K show a sharp isotropic signal at g = 2.0043 along with signals for the Cu(II) component. An illustrative spectrum for the case of complex **1·MeOH** is presented in Fig. 10. This isotropic signal at g = 2.0043 undoubtedly proves the generation of the radical intermediate. Further, the signal intensity of the radical species depends on the temperature and the radical signal at g = 2.0043 completely disappeared at 77 K (Fig. S21, ESI†). This characteristic probably leads to the valence tautomerization between $\{\mathbf{Cu^{II}}\text{–}\mathbf{(AP^{Ph,t\text{-}Bu})^{2-}}\}$ and $\{\mathbf{Cu^{I}}\text{–}\mathbf{(ISQ^{Ph,t\text{-}Bu})^{\bullet -}}\}$ as shown in Fig. 11. Such thermally induced valence tautomerism has been reported for catecholate and 2-amidophenoxide based metal complexes in the literature.[33] Therefore, these results indicate that the complex–substrate adduct exists in two electronic states *viz* "Cu^{II}–2-amido-phenolato" and "Cu^{I}–2-iminosemiquinonato radical anion" by valence tautomerism. Such a "Cu^{I}–(substrate radical)" intermediate is believed to be responsible for activating molecular dioxygen.

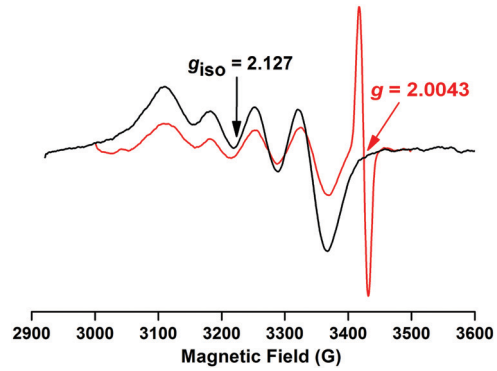

Fig. 10 X-Band EPR spectra of complex **1·MeOH** (1 mM; black line) and after treating with 2-anilino-4,6-di-*tert*-butylphenol (10 mM; red line) at 298 K in methanol. Microwave frequency = 9.60542 GHz, microwave power = 15 mW, modulation frequency = 5 kHz, modulation amplitude = 3 G.

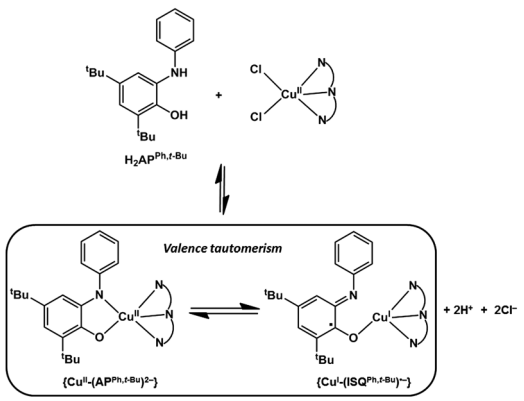

Fig. 11 Substrate–complex adduct formation in the reaction of the copper(II) complexes with 2-anilino-4,6-di-*tert*-butylphenol ($H_2AP^{Ph,t\text{-}Bu}$) and valence tautomerism. N–N–N represents tridentate ligand L^1 or L^2 or L^3 for complexes **1·MeOH** or **2·H₂O** or **3**, respectively. The four coordination sites as shown in copper(I) species are tentatively assigned.

Effects of temperature and pH on the reaction rates

As demonstrated above with $H_2AP^{Ph,t\text{-}Bu}$ it is clear that the extent of valence tautomerism in the complex–substrate adduct depends on temperature. At higher temperature the equilibrium shifts towards the reactive "Cu^{I}–(substrate radical)" tautomeric form, which presumably activates dioxygen. Since both substrates H_2AP and $H_2AP^{Ph,t\text{-}Bu}$ consist of a common chromophore group, it is reasonable to assume that a similar situation would prevail for H_2AP as well. Therefore, a temperature dependence of the rate of reaction is likely to be expected. In order to see the thermal effect on the rate of aerial oxidation of H_2AP, kinetic experiments were performed with all the complexes at various temperatures (298–313 K), under the experimental conditions employed in the

Table 4 Activation parameters for the aerial oxidation of H_2AP by copper(II) complexes

Complex	E_a (kJ mol^{-1})	$\Delta H^{\ddagger}$ (kJ mol^{-1})	$\Delta S^{\ddagger}$ (J mol^{-1} K^{-1})
1·MeOH	46.18	44.20	−152
2·H$_2$O	43.54	40.45	−164
3	36.68	33.58	−185

kinetic experiments. As observed, the reaction rate increases with an increase in temperature in all three catalytic reactions, validating our assumption. The activation parameters E_a, $\Delta H^{\ddagger}$, and $\Delta S^{\ddagger}$ (Table 4) were obtained from Arrhenius (Fig. S22, ESI†) and Eyring (Fig. S23, ESI†) plots. The activation energies for the catalytic reactions performed by **1·MeOH**, **2·H$_2$O** and **3** are in accordance with the observed trend of the reaction rates. Notably, in all three cases $\Delta S^{\ddagger}$ is negative, indicating that substrate–complex association occurs at the transition state.

The pH dependence of the catalytic activities was investigated in the pH range 7.5–9.6. Since the aerial oxidation of H_2AP to APX also involves release of protons, the rate of reaction is highly influenced by the pH of the medium for all three catalytic reactions. As shown in Fig. S24 (ESI†), the reaction rate increases with an increase in pH, giving rise to a sigmoid shape curve.[34]

Mass spectrometry measurements of reaction intermediates

HRMS-ESI spectroscopy was employed to identify the reaction intermediates during the course of catalytic oxidation. In a typical experiment, one equivalent of copper(II) complex and ten equivalents of H_2AP were mixed together in methanol–water and the reaction solution was injected (within 5 minutes) into the mass spectrometer. The spectra are displayed in Fig. S25–S27 (ESI†). The ESI spectrum of the reaction solution for **1·MeOH** exhibited peaks at *m/z* 404.0691, 459.0867 and 493.0959, corresponding to ions $[Cu(L^1)(HAP)]^+$ (calc. *m/z* 404.0698), $\{[Cu(L^1)(HAP)]^+ + CH_3OH + Na^+ + e^-\}^+$ (calc. *m/z* 459.0858) and $\{[Cu(L^1)(HAP)(Cl)] + CH_3OH + Na^+\}^+$ (calc. *m/z* 493.0547), respectively. These observations clearly establish the formation of a complex–substrate adduct at the initial step of the catalytic reaction. In addition to that a peak at *m/z* 564.9997 was observed. This peak can be attributed to the $\{[Cu(L^1)(AP')] + CH_3OH + Na^+\}^+$ (calc. *m/z* 565.1151) ion where H_2AP' corresponds to the protonated form of a reactive intermediate generated *via* coupling between 2-benzoquinone monoamine (BQMI) and H_2AP during the course of the catalytic reaction (*vide infra*). This finding clearly shows that H_2AP' may further bind to the copper centre as a substrate in subsequent steps of the oxidation process. In the reaction solution of complex **2·H$_2$O** a peak was observed at *m/z* 252.1130 that can be assigned as a water cluster of free H_2AP', $\{H_2AP'(H_2O)_2 - e^-\}^+$ (calc. *m/z* 252.1110). Other peaks related to an AP-bound adduct were observed at *m/z* 506.1270, 565.1394 and 601.1645, which can be assigned as $\{[Cu(L^2)(AP)] + CH_3OH + H_2O - e^-\}^+$ (calc. *m/z* 506.1253), $\{[Cu(L^2)(HAP)_2] - e^-\}^+$ (calc. *m/z* 565.1413), and $\{[Cu(L^2)(HAP)_2] + 2H_2O - e^-\}^+$ (calc. *m/z* 601.1625), respectively. It should be noted here that the assignment of the latter two peaks (*m/z* 565.1394 and 601.1645) is not straightforward as these two peaks can also be assigned as an AP′-bound adduct such as $\{[Cu(L^2)(HAP')]^+ + H^+ + e^-\}^+$ (calc. *m/z* 565.1413), and $\{[Cu(L^2)(HAP')]^+ + 2H_2O + H^+ + e^-\}^+$ (calc. *m/z* 601.1625), respectively. Considering the plausible formation of H_2AP' *in situ* during the reaction as well as its detection in ESI-MS, the assignment of those two signals as an AP′-bound adduct cannot be ruled out. In the spectrum for complex **3**, the signal for H_2AP' was also observed as a sodium aggregate $\{H_2AP' + Na^+\}^+$ at *m/z* 239.1292 (calc. 239.0796). The peak observed at *m/z* 538.1650 can also be assigned to a complex–substrate adduct of either type $\{[Cu(L^3)(HAP)_2] + Na^+\}^+$ or $\{[Cu(L^3)(HAP')]^+ + H^+ + Na^+ + 2e^-\}^+$ (calc. *m/z* 538.1154).

Discussion on a plausible mechanism

The experimental results discussed above point toward the conclusion that the aerial oxidation of H_2AP to APX performed by complexes **1·MeOH**, **2·H$_2$O** and **3** occurs through a common mechanistic pathway. Fig. 12 shows the oxidative cascade mediated by the copper(II) complexes. The overall six-electron oxidation is proposed to occur in a series of three consecutive two-electron transfer processes. From stoichiometry determination it is obvious that two molecules of dioxygen are required as a terminal oxidant for formation of one molecule of APX. Based on the kinetics and other experimental findings these three oxidative steps may be described as stated below.

Step I. In the very first step H_2AP coordinates with the copper(II) centre by replacing the labile chloride ions as evidenced from mass spectroscopy. The deprotonated form of H_2AP (coordination induced deprotonation) forms a stable complex–substrate adduct, since the rate of reaction is highly dependent on the pH of the medium. Coordination of AP^{2-} to the copper(II) centre may be monodentate or bidentate; however, considering the chelate effect the bidentate mode is preferred. The saturation kinetics implies that the complex–substrate adduct exists in equilibrium with its constituent reactants. The reactive $\{\mathbf{Cu^{I}}\text{–}\mathbf{(ISQ)^{\bullet -}}\}$ tautomer can be generated from $\{\mathbf{Cu^{II}}\text{–}\mathbf{(AP)^{2-}}\}$ by valence tautomerism. These two redox isomers may also exist in equilibrium as demonstrated by EPR spectroscopy. In a successive step dioxygen irreversibly oxidises $\{\mathbf{Cu^{I}}\text{–}\mathbf{(ISQ)^{\bullet -}}\}$ species to produce 2e$^-$ oxidised product BQMI. This oxidation process might have propagated *via* generation of a superoxide intermediate that finally produces H_2O_2 with concomitant regeneration of the catalyst in the copper(II) state (Fig. S28, ESI†). The highly electrophilic BQMI then rapidly couples with another molecule of H_2AP to form H_2AP'. The detection of signals for H_2AP' in mass spectrometry supports its formation during the catalytic process.

Step II. In a follow up step H_2AP' binds with the copper(II) centre (tentatively in a similar fashion to that of H_2AP) to produce a new complex–substrate intermediate, as supported by mass spectral studies. Following a similar reaction sequence to that shown in step I, the $\{\mathbf{Cu^{I}}\text{–}\mathbf{(ISQ')^{\bullet -}}\}$ species would be generated from the new complex–substrate intermediate $\{\mathbf{Cu^{II}}\text{–}\mathbf{(AP')^{2-}}\}$ by valence tautomerism. This reactive $\{\mathbf{Cu^{I}}\text{–}\mathbf{(ISQ')^{\bullet -}}\}$ species then undergoes irreversible 2e$^-$ oxidation in the presence

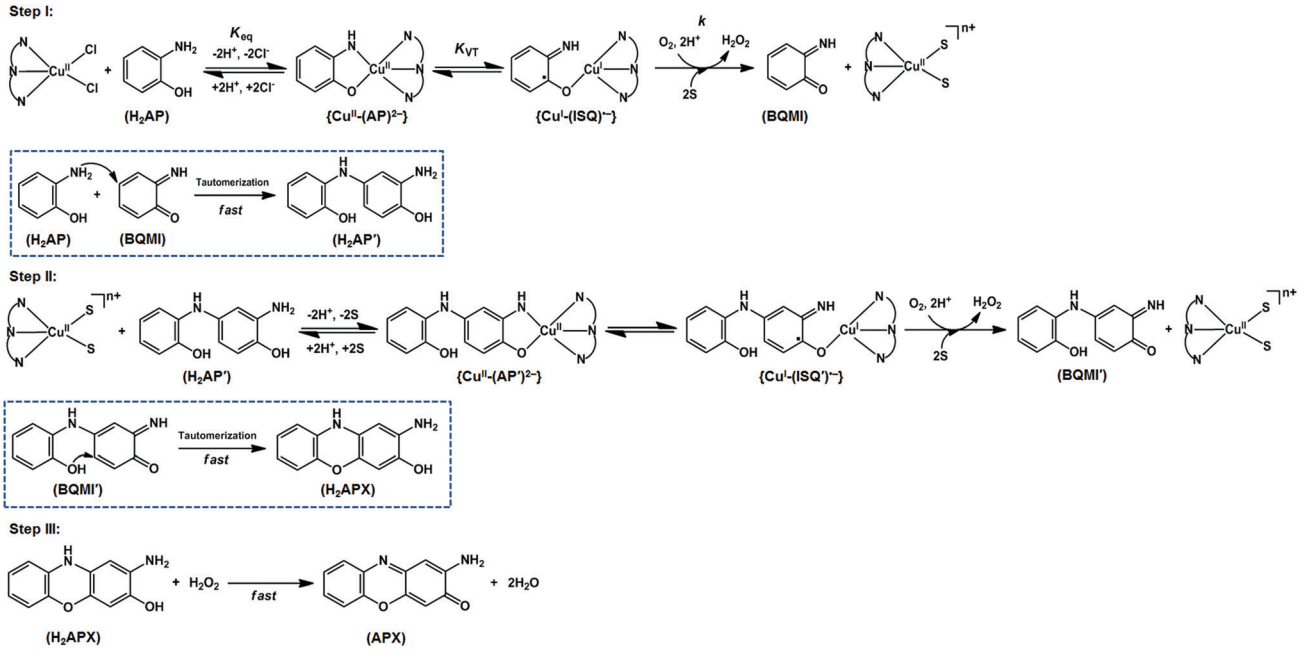

Fig. 12 Plausible reaction pathway of formation of 2-amino-phenoxazine-3-one (APX) from 2-aminophenol (H_2AP) catalysed by copper(II) complexes. N–N–N represents tridentate ligand L^1 or L^2 or L^3 for complexes **1·MeOH** or **2·H₂O** or **3**, respectively. The four coordination sites as shown in copper(I) species are tentatively assigned. S represents Cl^-/water/methanol and *n* varies from 0 to 2 depending on the types of ligand, S.

of molecular dioxygen to produce reactive intermediate BQMI′. Successively, BQMI′ rapidly transforms to cyclic product H_2APX *via* facile tautomerization. In this course of the reaction H_2O_2 is likely to be generated and the catalyst comes back to the copper(II) state.

Step III. In the final step the four-electron oxidised product H_2APX probably leaves the catalyst and being an activated compound it can be easily oxidised by H_2O_2 to the final product 2-amino-phenoxazine-3-one (APX). Thus the final two-electron oxidation may take place without involvement of the catalyst. A similar proposition for the final two-electron transfer process was also made for the enzyme system as demonstrated by Begley *et al.*[10] Therefore, in a single catalytic cycle one mole of H_2O_2 would be formed as a by-product per mole of APX formation. Iodometric titrations confirmed the formation of H_2O_2 in an equal amount to APX, supporting our proposed reaction pathways.

From the above discussion it is obvious that step III cannot be a rate determining step since the formation of APX shows first order dependence with respect to the catalyst concentration. Therefore, the irreversible oxidation of complex–substrate adducts by dioxygen in either step I or step II might be the rate determining step. H_2AP', being more electron-rich in nature, is likely to be more easily oxidised than H_2AP. So we believe that the formation of BQMI *via* irreversible oxidation of $\{\mathbf{Cu^I}\text{–}\mathbf{(ISQ)^{\bullet -}}\}$ by dioxygen in step I is the slowest step in the overall catalytic cycle, wherein complex–substrate adduct formation, valence tautomerism and dioxygen activation are three important aspects of the reaction. In previous reports also the initial activation of the H_2AP molecule to form the radical species or iminobenzoquinone (BQMI) has been proposed as the rate limiting step.[13,15c,21f] So, the kinetic pattern shown in step I can be described by the rate law in eqn (2) (see the ESI†):

$$v_0 = \frac{kK_{eq}K_{VT}[\text{catalyst}]_0[H_2AP]_0}{1 + K_{eq}[H_2AP]_0 + K_{eq}K_{VT}[H_2AP]_0} \quad (2)$$

where k is the rate constant, which includes all other pseudo stationary parameters, such as $[O_2]$ *etc.*; K_{eq} and K_{VT} are the equilibrium constants to produce the complex–substrate adduct and valence tautomers, respectively; and $[\text{catalyst}]_0$ and $[H_2AP]_0$ are the initial concentrations of the added copper(II) complex and 2-aminophenol, respectively. It is assumed that the decrease of the initial concentration of H_2AP is negligible at the early stage of the reaction. The rate constant k and equilibrium constants K_{eq} and K_{VT} have been determined by nonlinear least squares fitting of eqn (2) to the plots of v_0 *vs.* $[H_2AP]_0$ for all three catalytic reactions (see Fig. S29, ESI,† and Table 5). The rate constant (k) values calculated from eqn (2) for all three reactions are in good agreement with the values obtained from the slope of straight lines of v_0 *vs.* $[\text{complex}]_0$ plots, providing additional support for kinetic eqn (2) and the proposed reaction pathway.

Table 5 Rate and equilibrium constants determined from the fitting of eqn (2) to the plots of v_0 *vs.* $[H_2AP]_0$

Complex	K_{eq} (M^{-1})	K_{VT}	k (s^{-1})
1·MeOH	867	6.90	166×10^{-5}
2·H₂O	932	7.10	203×10^{-5}
3	2296	7.20	222×10^{-5}

Lastly, it should be noted that H_2AP may compete with H_2AP' towards binding with the copper(II) centre in step II. If H_2AP' cannot bind effectively suppression of catalysis may be anticipated. In fact a lower degree of APX formation was observed at a very high concentration of the substrate ($[H_2AP]_0/[complex]_0 > 100$), supporting the hypothesis. Such a kind of inhibition effect of H_2AP may be avoided by designing a multi-metallic catalyst where cooperativity among metal centres may facilitate the binding of various substrates. So, nature's strategy of designing a multi-copper active site for efficient PHS activity may be realized.

Summary and conclusions

In the present work, we report the synthesis and characterizations of three mononuclear copper(II) complexes **1·MeOH**, **2·H_2O** and **3** supported with Schiff base N_3 donor ligands with variable donor moieties. The respective Schiff base ligands were derived *in situ via* oxidative dehydrogenation during metalation from their reduced Schiff base derivatives. The phenoxazinone synthase-like activities of all three complexes were investigated following the aerial oxidation of 2-aminophenol (H_2AP) to 2-amino-phenoxazine-3-one (APX) in methanol–water (pH 8.6) solvent. The present study reveals a structure–function relation of the catalytic reactivity. In the mechanistic interpretation the finding of valence tautomerism in a complex–substrate adduct (as demonstrated by EPR spectroscopy especially with 2-anilino-4,6-di-*tert*-butylphenol as a substrate) and thereby generation of a reactive "Cu^{I}–(substrate radical)" intermediate responsible for activating molecular dioxygen is a noteworthy result. Based on ESI-MS data, kinetic analysis and the stoichiometry of the reaction a plausible reaction pathway has been proposed, where the overall six-electron transfer occurs in a series of three consecutive two-electron transfer pathways. Thus, the results presented here are of significance in understanding phenoxazinone synthase-like activity.

Conflicts of interest

There are no conflicts to declare.

Acknowledgements

S. M. gratefully acknowledges the financial support from Science and Engineering Research Board (SERB), Government of India (Ref.: EMR/2015/001136); DST-INSPIRE Faculty award, Government of India (Ref.: DST/INSPIRE Faculty Award/IFA12-CH-72); and ISIRD start-up research grant, IIT Kharagpur (Ref.: IIT/SRIC/CHY/SMR/2015-16/60). N. P. thanks IIT Kharagpur for a PhD fellowship. We thank the Department of Science and Technology (DST), Government of India, under the DST-FIST programme for the NMR (SR/FST/CSII-026/2013) facility. We thank the Department of Chemistry and Central Research Facility, IIT Kharagpur, for providing infrastructural and instrumental facilities.

References

1 T. Punniyamurthy, S. Velusamy and J. Iqbal, *Chem. Rev.*, 2005, **105**, 2323–2363.
2 O. A. Kholdeeva and O. V. Zalomaeva, *Coord. Chem. Rev.*, 2016, **306**, 302–330.
3 Y.-F. Liang and N. Jiao, *Acc. Chem. Res.*, 2017, **50**, 1640–1653.
4 P. Gandeepan, T. Muller, D. Zell, G. Cera, S. Warratz and L. Ackermann, *Chem. Rev.*, 2019, **119**, 2192–2452.
5 R. Trammell, K. Rajabimoghadam and I. Garcia-Bosch, *Chem. Rev.*, 2019, **119**, 2954–3031.
6 C. E. Elwell, N. L. Gagnon, B. D. Neisen, D. Dhar, A. D. Spaeth, G. M. Yee and W. B. Tolman, *Chem. Rev.*, 2017, **117**, 2059–2107.
7 (*a*) E. A. Lewis and W. B. Tolman, *Chem. Rev.*, 2004, **104**, 1047–1076; (*b*) L. M. Mirica, X. Ottenwaelder and T. D. P. Stack, *Chem. Rev.*, 2004, **104**, 1013–1045.
8 A. De, S. Mandal and R. Mukherjee, *J. Inorg. Biochem.*, 2008, **102**, 1170–1189.
9 C. E. III Barry, P. G. Nayar and T. P. Begley, *J. Am. Chem. Soc.*, 1988, **110**, 3333–3334.
10 C. E. III Barry, P. G. Nayar and T. P. Begley, *Biochemistry*, 1989, **28**, 6323–6333.
11 J. C. Freeman, P. G. Nayar, T. P. Begley and J. J. Willafranca, *Biochemistry*, 1993, **32**, 4826–4830.
12 A. W. Smith, A. Camara-Artigas, M. Wang, J. P. Allen and W. A. Francisco, *Biochemistry*, 2006, **45**, 4378–4387.
13 S. K. Dey and A. Mukherjee, *Coord. Chem. Rev.*, 2016, **310**, 80–115.
14 C. Mukherjee, T. Weyhermuller, E. Bothe, E. Rentschler and P. Chaudhuri, *Inorg. Chem.*, 2007, **46**, 9895–9905.
15 (*a*) M. Mitra, T. Kundu, G. Kaur, G. Sharma, A. R. Choudhury, Y. Singh and R. Ghosh, *RSC Adv.*, 2016, **6**, 58831–58838; (*b*) S. Sagar, S. Sengupta, A. J. Mota, S. K. Chattopadhyay, A. E. Ferao, E. Riviere, W. Lewis and S. Naskar, *Dalton Trans.*, 2017, **46**, 1249–1259; (*c*) O. V. Nesterova, O. E. Bondarenko, A. J. L. Pombeiro and D. S. Nesterov, *Dalton Trans.*, 2020, **49**, 4710–4724.
16 (*a*) P. Mahapatra, S. Ghosh, S. Giri, V. Rane, R. Kadam, M. G. B. Drew and A. Ghosh, *Inorg. Chem.*, 2017, **56**, 5105–5121; (*b*) P. Mahapatra, M. G. B. Drew and A. Ghosh, *Cryst. Growth Des.*, 2017, **17**, 6809–6820; (*c*) S. Dutta, J. Mayans and A. Ghosh, *Dalton Trans.*, 2020, **49**, 1276–1291.
17 (*a*) A. K. Ghosh, A. Ali, Y. Singh, C. S. Purohit and R. Ghosh, *Inorg. Chim. Acta*, 2018, **474**, 156–163; (*b*) D. Mondal, A. K. Ghosh, A. Chatterjee and R. Ghosh, *Inorg. Chim. Acta*, 2019, **486**, 719–723; (*c*) T. Dutta, S. Mirdya, P. Giri and S. Chattopadhyay, *Polyhedron*, 2020, **175**, 114164; (*d*) S. Roy, T. Dutta, M. G. B. Drew and S. Chattopadhyay, *Polyhedron*, 2020, **178**, 114311; (*e*) P. K. Mudi, N. Bandopadhyay, M. Joshi, M. Shit, S. Paul, A. R. Choudhury and B. Biswas, *Inorg. Chim. Acta*, 2020, **505**, 119468.
18 (*a*) T. Horvath, J. Kaizer and G. Speier, *J. Mol. Catal. A: Chem.*, 2004, **215**, 9–15; (*b*) M. R. Maurya, S. Sikarwar, T. Joseph and S. B. Halligudi, *J. Mol. Catal. A: Chem.*, 2005, **236**, 132–138; (*c*) B. Chowdhury, M. Maji and B. Biswas, *J. Chem. Sci.*, 2017, **129**, 1627–1637; (*d*) W. P. Sohtun, S. Muthuramalingam, M. Velusamy and R. Mayilmurugan, *Inorg. Chem. Commun.*,

2019, **110**, 107608; (*e*) A. E.-M. M. Ramadan, S. Y. Shaban, M. M. Ibrahim, A. A.-H. Abdel-Rahman, S. A. Sallam, S. A. Al-Harbi and W. Omar, *New J. Chem.*, 2020, **44**, 6331–6345.

19 (*a*) I. C. Szigyarto, T. M. Simandi, L. I. Simandi, L. Korecz and N. Nagy, *J. Mol. Catal. A: Chem.*, 2006, **251**, 270–276; (*b*) C. Mukherjee, T. Weyhermuller, E. Bothe and P. Chaudhuri, *C. R. Chim.*, 2007, **10**, 313–325; (*c*) J. Kaizer, G. Barath, R. Csonka, G. Speier, L. Korecz, A. Rockenbauer and L. Parkanyi, *J. Inorg. Biochem.*, 2008, **102**, 773–780; (*d*) A. Panja, *Polyhedron*, 2014, **79**, 258–268; (*e*) A. Panja, *RSC Adv.*, 2014, **4**, 37085–37094; (*f*) S. C. Kumar, A. K. Ghosh, J.-D. Chen and R. Ghosh, *Inorg. Chim. Acta*, 2017, **464**, 49–54.

20 (*a*) T. M. Simandi, L. I. Simandi, M. Gyor, A. Rockenbauer and A. Gomory, *Dalton Trans.*, 2004, 1056–1060; (*b*) M. Ismael, A.-M. M. Abdel-Mawgoud, M. K. Rabia and A. Abdou, *Inorg. Chim. Acta*, 2020, **505**, 119443.

21 (*a*) L. I. Simandi, T. Barna and S. Nemeth, *J. Chem. Soc., Dalton Trans.*, 1996, 473–478; (*b*) A. Panja, M. Shyamal, A. Saha and T. K. Mandal, *Dalton Trans.*, 2014, **43**, 5443–5452; (*c*) A. Panja, *Dalton Trans.*, 2014, **43**, 7760–7770; (*d*) M. Mahato, D. Mondal and H. P. Nayek, *ChemistrySelect*, 2016, **2**, 6777–6782; (*e*) K. Ghosh, K. Harms and S. Chattopadhyay, *ChemistrySelect*, 2017, **2**, 8207–8220; (*f*) N. C. Jana, M. Patra, P. Brandao and A. Panja, *Polyhedron*, 2019, **164**, 23–34.

22 (*a*) A. Kumar, A. Sengupta, S. Demeshko and R. Mukherjee, *Polyhedron*, 2019, **172**, 226–235; (*b*) P. Chaudhuri, C. N. Verani, E. Bill, E. Bothe, T. Weyhermuller and K. Wieghardt, *J. Am. Chem. Soc.*, 2001, **123**, 2213–2223.

23 S. Stoll and A. Schweiger, *J. Magn. Reson.*, 2006, **178**, 42–55.

24 G. Kinunda and D. Jaganyi, *Transition Met. Chem.*, 2014, **39**, 451–459.

25 (*a*) G. M. Sheldrick, *Acta Crystallogr., Sect. A: Found. Adv.*, 2015, **71**, 3–8; (*b*) L. J. Farrugia, *WINGX Version 2014.1. An Integrated Systems of Windows programs for the solution, Refinement and Analysis of Single-Crystal X-ray Diffraction Data*, Department of Chemistry, University of Glasgow, Glasgow, UK, 2014.

26 R. G. Bates, M. Paabo and R. A. Robinson, *J. Phys. Chem.*, 1963, **67**, 1833–1838.

27 L. Gasque, A. Mendieta and G. Ferrer-Sueta, *Dalton Trans.*, 2020, **49**, 3365–3368.

28 S. Mandal, J. Mukherjee, F. Lloret and R. Mukherjee, *Inorg. Chem.*, 2012, **51**, 13148–13161.

29 (*a*) A. Bottcher, H. Elias, E.-G. Jager, H. Langfelderova, M. Mazur, L. Muller, H. Paulus, P. Pelikan, M. Rudolph and M. Valko, *Inorg. Chem.*, 1993, **32**, 4131–4138; (*b*) R. Klement, F. Stock, H. Elias, H. Paulus, P. Pelikan, M. Valko and M. Mazur, *Polyhedron*, 1999, **18**, 3617–3628.

30 A. W. Addison, T. N. Rao, J. Reedijk, J. V. Rijn and G. C. Verschoor, *J. Chem. Soc., Dalton Trans.*, 1984, 1349–1356.

31 (*a*) R. Mukherjee, Copper. in *Comprehensive Coordination Chemistry II: From Biology to Nanotechnology*, ed. J. A. McCleverty, T. J. Meyer and D. E. Fenton, Elsevier/Pergamon, Amsterdam, 2004, vol. 6, pp. 747–910; (*b*) in *Comprehensive Coordination Chemistry*, ed. B. J. Hathaway and G. Wilkinson, Pergamon, New York, 1987, vol. 5, pp. 533–774.

32 J. H. Espenson, *Chemical Kinetics and Reaction Mechanism*, McGraw-Hill, 1995, 70–100.

33 A. Rajput, A. K. Sharma, S. K. Barman, A. Saha and R. Mukherjee, *Coord. Chem. Rev.*, 2020, **414**, 213240.

34 A sigmoidal curve fitting (Origin version 6.0) of the dependence of initial rates on pH was performed to determine the kinetic pK_a values. The pK_a values were determined to be 8.62 for **1·MeOH**, 8.58 for **2·H$_2$O** and 8.40 for **3**.